ISSN 0915-633X

NATIONAL INSTITUTE FOR FUSION SCIENCE

Effect of Continuous Eigenvalue Spectrum on Plasma Transport in Toroidal Systems

T. Yamagishi

(Received – Feb. 18, 1993)

NIFS-214 Mar. 1993

RESEARCH REPORT
NIFS Series

NAGOYA, JAPAN

Effect of Continuous Eigenvalue Spectrum on Plasma Transport in Toroidal Systems

Tomejiro Yamagishi
Fukui Institute of Technology, Gakuen Fukui 910

Abstract

The effect of the continuous eigenvalue of the Vlasov equation on the cross field ion thermal flux is investigated. The continuum contribution due to the toroidal drift resonance is found to play an important role in ion transport particularly near the edge, which may apply to the interpretation of the sharp increase of ion heat conductivity near the periphery observed in large tokamaks.

Keywords: Ion temperature gradient drift mode, Vlasov continuum, ion toroidal drift resonance, cross field ion thermal flux, edge phenomenon, gyro-Bohm diffusion coefficient, frequency power spectrum, electrostatic turbulence, transit resonance continuum

§1. Introduction

The ion heat conductivity observed in toroidal fusion experimental devices is larger than the heat conductivity predicted by neoclassical theory by more than one order of magnitude[1]~[3]. Numerous studies on the anomalous ion heat conductivity have been made based on the ion temperature gradient drift mode[4]~[8]. The most simple and most frequently used method to evaluate the anomalous diffusion coefficient $D_\perp$ is to apply the formula $D_\perp=\gamma/k_\perp^2$ derived from the balance condition between the growth rate of certain micro-instability and the damping rate $-k_\perp^2 D_\perp$ due to the anomalous diffusion[9], where $k_\perp$ is the perpendicular wave number of the instability. The above mixing length formula is some times successful to some extent to interprete experimentally observed transport phenomenon.

The difficulty with the theory based on the linear instability is that the electric and/or magnetic fluctuations which are obviously correlated to the instability are usually not observed. Furthemore, experimentally observed transport coefficient does not change at the onset of the instability predicted by the thoery.

The mixing length theory relays on the existence of certain linear instability or discrete eigenvalue γ derived from the dispersion relation. In addition to the discrete eigenvalue, it is well known that the basic Vlasov equation has the continous eigenvalue[10]~[12]. The existence of the continous eigenvalue induced by the wave-particle resonance condition is one of the most significant characteristics of the Vlasov equation.

Since the continuum extends on the real axis in the complex ω-plane, it may by considered as the continously infinite set of steady oscillating modes. Case[11] applied Van Kampen's theory[10] to the Vlasov type neutron transport equation, and constracted the orthogonal complete set of eigenfunctions corresponding to the discrete and continous eigenvalues for the Vlasov equation. In neutron transport theory, the contribution from the discrete eigenvalue corresponds to the solution of the diffusion equation which describes the random walk process of particles, while the continuum contribution corresponds to

the free flight of particle without collision. The continuum contribution may also describes the spatial transient phenomenon, which plays an important role near a source or boundary.

In the field of neutron transport theory, the transport theory means that both discrete and continuous eigen modes are included, in which the major difficulty is in the treatment of the continuum contribution. The transport theory, therefore, is distinctly different from the diffusion theory where only particle random walk process is taken into account. Since the basic equations for neutron transport and plasma kinetics are the same Vlasov equation, the importance of the continuum contribution in neutron transport process may be true also in the field of plsma dynamics. It is the purpose of this paper, therefore, to investigate the effect of continuum contribution to the radial plsama transport in toroidal systems assuming the power spetrum of electric field fluctuation is given.

§2. Eigenvalue Spetrum of Ion Temperature Gradient Mode

We start with the solution of the first order perturbation of gyrokinetic equation of the form

$$f = J_0(\alpha)\frac{\omega-\omega_{*T}}{\omega-\omega_D-\omega_t}F_M\frac{e\phi}{T_i} \tag{1}$$

where all notations are standard as defined in Ref.(5): $\omega_D=-\omega_D(v_\perp^2/2+v_\parallel^2)$, $\omega_D=2\varepsilon_n\omega^*/\tau$, $\tau=T_e/T_i$, $\omega_t=k_\parallel v_\parallel$, $\varepsilon_n=L_n/R$, $1/L_n=-d\ln n/dr$, $\omega^*_T=\omega^*_e(1+\eta_i(v_\perp^2+v_\parallel^2-3/2))/\tau$, $\eta_i=d\ln T/d\ln n$, $\omega^*_e=k_y cT_e/eBL_n$, and quantities without index i stand for ion. Introducing eq.(1) into the quasi-neutrality condition

$$(1+\frac{1}{\tau})\varphi(\theta)=\int d^3v J_o(\alpha) f \tag{2}$$

yields the electrostatic local mode dispersion relation

$$D_{es}\equiv 1+\frac{1}{\tau}-\int d^3v\frac{\omega-\omega_{*T}}{\omega-\omega_D-\omega_t}J_o^2(\alpha)F_M=0 \tag{3}$$

The solution of $D_{es}(\omega_o)=0$ gives the discrete eigenvalue ω_o.

If we assume ω_D is a constant with respect to velocity, eq.(3) can be expressed in terms of the plasma dispersion function $Z(\zeta)$, and approximate solution may be derived for the eigenvalue ω. In this

approach, however, the correct η_i-mode is never obtained. To investigate the toroidal η_i-mode correctly, the velocity dependence of ω_D is essential, and we cannot assume ω_D as a constant. For the Maxwellian plasma, by neglecting trapped particles, eq.(1) can be written in the form of double integral:

$$D_{es}(\omega) \equiv 1+\frac{1}{\tau}-\frac{2}{\sqrt{\pi}}\int_0^\infty dx x e^{-x^2} J_o^2(\alpha)\int_{-\infty}^{\infty} dy \frac{\omega-\omega_*(1+\eta_i(x^2+y^2-3/2))}{\omega-\omega_D(x^2/2+y^2)-\omega_{ti}Y} e^{-y^2}=0 \qquad (4)$$

where $\alpha=(2b)^{1/2}x$ and $b=(k_\perp\rho_i)^2/2$.

In the fluid limit, eq.(4) may be solved by expanding the integrand in eq.(4) in terms of ω_D/ω and carrying out moment integrals for $\omega_D<<\omega$. This approach may give the interchange type solution $\omega_O=(\omega_*\omega_D\eta_i)^{1/2}$ when η_i is large enough[5]. Near the marginal state, however, the resonance effect becomes important, and the validity of this fluid approximation is broken down. To obtain the correct discrete eigenvalue of the η_i-mode, eq.(4) has been solved numerically by making use of conformal mapping method[13].

The double integral of the complex function in eq.(4) is time consuming particularly near the resonance condition: $\omega=\omega_D+k_{\parallel}v_{\parallel}$. If we neglect the transit ion, $k_{\parallel}=0$, and approximate the toroidal drift frequency in the form $\omega_D=\omega_D\bar{E}$ for the case without finite Larmor radius effect $b=0$, eq.(4) can be written in the form of single integral:

$$D_{es}(\omega) = 1+\frac{1}{\tau}-\frac{2}{\sqrt{\pi}}\int_0^\infty \frac{\omega-\omega_*(1+\eta_i(\bar{E}-3/2))}{\omega-\omega_D\bar{E}} e^{-\bar{E}}\bar{E}^{\frac{1}{2}} d\bar{E}=0 \qquad (5)$$

where $\bar{E}= E/T_i$. Numerical results of discrete eigenvalue ω_O obtained by solving eq.(5) are plotted in the complex ω-plane in Fig.1 for varous values of ε_n and η_i. As seen in Fig.1, as ε_n and/or η_i increases, the discrete eigenvalue tends to the negative real axis. This behavior is similar to the more acculate double integral dispersion relation[11].

The continuum on the negative real axis is the same as the continuously infinite set of the toroidal drift resonance condition:

$\omega=\omega_D E$ for $0<E<\infty$. That is, the negative real axis is the continuous eigenvalue spectrum of the solution (1) without transit ion. As ε_n and/or η_i increases, the discrete eigenvalue tends to this continuum and vanishes. The continuous eigenvalue spectrum may be considered as the continuously infinite set of steady oscillating modes. Since discrete mode and continuous modes are orthogenal to each other, the continuous eigenvalue does not affect the dispersion relation $Des(\omega_o)=0$. Although the continuum has no direct effect to the discrete mode or the η_i-mode stability, it may play an important role for plasma transport.

§3. Cross Field Ion Thermal Flux

We consider the effects of the discrete η_i-mode eigenvalue and the continuous eigenvalue on the cross field ion thormal flux defined by[14]

$$Q_i=\int d^3v\langle E\tilde{v}_x\tilde{f}\rangle \equiv -\chi_i n\frac{dT_i}{dr} \tag{6}$$

where $\tilde{v}_x$ is the radial component of ExB-drift velocity and the angular brackets represent the ensemble average. We apply the Fourier representation for the perterbation of the form

$$\tilde{f}=\sum_{k,\omega} f_{k\omega}\, e^{-i\omega t+ikr} \tag{7}$$

Introducing the Fourier representation of $\tilde{v}_x$ and $\tilde{f}$ in eq.(6), and applying the random phase approximation[15], we have the flux in the form

$$Q_i=\sum_{k,\omega}\int d^3v v_{k,\omega}^{*} f_{k\omega} E \tag{8}$$

Substitution of the velocity $v_{k\omega}{}^{*}=-ik_y c\phi/B$ and eq.(1) without $k_{\parallel}v_{\parallel}$ for $f_{k\omega}$ into eq.(8) we have

$$Q_i=\sum_{k,\omega}\left|\frac{e\phi}{T}\right|^2_{k,\omega} c\frac{k_y T_i}{eB} nT_i\hat{q}(k,\omega) \tag{9}$$

where $\hat{q}$ is the normelized flux defined by

$$\hat{q}_i^{o}\equiv -Im\int d^3v\frac{\omega_o-\omega_{*T}}{\omega_o-\omega_D}F_M\frac{E}{T_i}J_o^2(\alpha) \tag{10}$$

For the discrete η_i-mode eigenvalue $\omega_o=\omega_r+i\gamma$, the growth rate γ gives

the real ion heat flux:

$$\hat{q}_o = \int d^3v \frac{(\omega_D - \omega_{*T})\, r}{(\omega_r - \omega_D)^2 + r^2} J_o^2(\alpha) F_M \frac{E}{T_i} \qquad (11)$$

Far away form the marginal state, $\eta_i >> \eta_c$, the growth rate may be of the interchange type $\gamma = (\omega_* \omega_D \eta_i)^{1/2}$. For this η_i-mode, assuming $\omega_r << \gamma$ and $\omega_D << \omega_*$, we have form eq.(11) for b=0

$$\hat{q}_o = \left(\frac{\eta_i - \eta_c}{2\varepsilon_n} \right)^{\frac{1}{2}} \qquad (12)$$

The sum over the wave number k in eq.(9) is replaced by the maximum value: $|e\phi/T|^2/(k_\perp L)^{-2}$, which occurs in the range of $0.1 < k_\perp \rho_i < 0.3$ (14). For the discrete mode, the sum over the frequency is just replaced by the single terms. If we approximate the characterstic scale length L by $L = (RL_T)^{1/2}$ (5) the heat flux may be written in the form

$$Q_i = \lambda \frac{n T_i}{L_T} \frac{v_i \rho_i^2}{R} \hat{q}_o = -n \chi_i \frac{dT_i}{dr} \qquad (13)$$

where $1/L_T = -d\ln T_i/dr$, the constant λ depends on the value of $k_y \rho_i$, and χ_i is the ion heat conductivity. From eq.(13), we have the ion heat conductivity in term of $\hat{q}$:

$$\chi_i = \lambda \frac{v_i \rho_i^2}{R} \hat{q} \qquad (14)$$

Substitution of eq.(12) into eq.(14) yields the heat conductivity due to the discrete η_i-mode,

$$\chi_i^o = \lambda \frac{v_i \rho_i^2}{R} \left(\frac{\eta_i - \eta_c}{2\varepsilon_n} \right)^{\frac{1}{2}} \qquad (15)$$

where the coefficient λ is an adjustable parameter. Although eq.(15) is derived under many assumptions, the radial profile of eq.(15) was close to the heat conductivity calculated consistently(13) with the dispersion relation (5) removing assumptions $\omega_r << r$, $\omega_D << \omega_*$ and $\eta_i >> \eta_c$.

We now evaluate the continuum contribution to the thermal flux Q_i. In this case, the imaginary part due to the resonance, the second term of the formula

$$\frac{1}{\omega - \omega_D} = P \frac{1}{\omega - \omega_D} - i\pi\delta(\omega - \omega_D)$$

gives the real flux Q_i. We introduce the frequency power spectrum

function $S(\omega)$ for the fluctuations:

$$\left|\frac{e\phi}{T}\right|^2_{k,\omega} = \frac{1}{k_\perp^2 L^2} S(\omega) \tag{16}$$

where S must satisfies the normalization condition $\int d\omega S(\omega)=1$.

The sum over the frequency in eq.(9) should be replaced by an integral over the continuum $C=\{w| -\infty<\omega<0\}$. The continuum contribution to the flux can be written in the form

$$Q_i^C = \frac{nT_i}{k_\perp^2 L^2}\frac{cT_i}{eB}\hat{q}_c \tag{17}$$

where the normalized flux is defined by

$$\hat{q}_c = \int_C d\omega S(\omega)\int d^3v(\omega-\omega_{*T})J_o^2(\alpha)F_M\frac{E}{T_i}\delta(\omega-\omega_D) \tag{18}$$

If we apply the same approximation; $\omega_D=-\omega_D E/T_i$ as in the above, bearing in mind the relation

$$\int d^3v F_M ... = \frac{1}{\sqrt{\pi}}\int_0^1 \frac{d\lambda}{\sqrt{1-\lambda}}\int_0^\infty d\bar{E}\bar{E}^{\frac{1}{2}}e^{-\bar{E}} .... \tag{19}$$

We have

$$\hat{q}_c = \frac{\sqrt{\pi}\omega_{*e}}{\tau\omega_s}\left\{(\eta_i-2\varepsilon_n)I_{\frac{1}{2}} + (1-\frac{3}{2}\eta_i)I_{\frac{3}{2}}\right\} \tag{20}$$

where $\lambda=\mu B/E$, $\mu=Mv^2/2B$, and I_j is the moment defined by

$$I_j \equiv \omega_s\int_o^\infty dw S(-\omega_D w) w^{\frac{1}{2}+j} e^{-w}\int_o^1 \frac{d\lambda}{\sqrt{1-\lambda}} J_o^2(\sqrt{2b\lambda w}) \tag{21}$$

Here ω_S is the characteristic frequency which represents the width of frequency power spectrum $S(\omega)$.

The integral which represents the finite Larmor radius effect in eq.(21)

$$g(Z) = \int_o^1 \frac{d\lambda}{\sqrt{1-\lambda}} J_o^2(\sqrt{Z\lambda}) \tag{22}$$

may be approximated by $2J_o^2(Z^{1/2})$ when Z is small. For the sake of simplicity, however, in what follows we neglect the finite Larmor radies effect. In this case, $g(0)=2$.

§4. Example of Frequency Power Spectrum of Fluctuations

We now proceed to the evaluation of the flux $\hat{q}_c$ and heat conductivity χ_i for two different frequency spectrum functions $S(\omega)$.

Cut-off Power Spectrum

First we consider the simplest case of the cut-off type defined by

$$S(\omega)=\begin{cases}\dfrac{1}{2\omega_s} & \text{for } |\omega|\le\omega_s \\ 0 & \text{otherwise}\end{cases} \qquad (23)$$

In this case, the moment integral defined by eq.(21) becomes

$$I_j=\int_0^{\frac{\omega_s}{\omega_b}} w^{2\left(\frac{1}{2}+j\right)} e^{-w} dw . \qquad (24)$$

In the case of the white noise, $ws\to\infty$, eq.(24) reduces to $I_0=\pi^{1/2}/2$, $I_1=3I_0/2$ and $I_2=5I_1/2$. However, from eq.(20), $\hat{q}_c\to 0$ as $\omega_s\to\infty$. Since the integrand in eq.(24) decays fast as w becomes large, the integrals I_j can be approximated by the infinite integrals as shown in the above even when ω_s is finite. For $\omega_s/\omega_D>3$, the moments are almost the same as the infinite integrals. Therefore, if we set the width of frequency spectrum as $\omega_s=3\omega_D$, eq.(20) yields

$$\hat{q}_c=\frac{\sqrt{\pi}}{4\varepsilon_n}(\eta_i+1-5\varepsilon_n) \qquad (25)$$

The inward transport contribution $-5\varepsilon_n$ in the brackets in eq.(25) comes from the first term in the factor $\omega-\omega_{*T}$ in eq.(18). When the continuum C extends to the whole real axis, this term vanishes. The nonvanishing of this inward transport term, therefore, is due to the characteristic of ion toroidal drift resonance.

If we assume a different kind of spectrum width: $\omega_s=\omega_*/\tau$, then the integral limit in eq.(24) becomes $\omega_s/\omega_D=1/2\varepsilon_n$. In this case too, when $2\varepsilon_n\ll 1$, I_j may be approximated by the infinite integral, and eq.(20) yields

$$\hat{q}_c=\frac{3}{4}\pi(\eta_i+1-5\varepsilon_n) \qquad (26)$$

Near the plasma boundary, $\varepsilon_n\ll 1$. Therefore eq.(26) may be applicable for the plasma edge. As seen in eqs.(25) and (26) depending on the spectrum width ω_s, the functional form of the continuum contribution $\hat{q}_c$ changes.

Gaussian power spectrum

Let us consider the Gaussian type power spectrum defined by

$$S(\omega)=\frac{1}{\omega_s\sqrt{\pi}}\exp\left(-\left(\frac{\omega}{\omega_s}\right)^2\right) \qquad (27)$$

In this case, from eq.(21) for b=0, we have the moment integral

$$I_j=\frac{1}{\sqrt{\pi}}\int_0^\infty dw w^{\frac{1}{2}+j}e^{-w}\exp\left(-\left(\frac{\omega_p}{\omega_s}\right)^2 w^2\right) \qquad (28)$$

Values of moments I_1 and I_2 sharply decrease as the spectrum width ω_D/ω_S increases.

When $\omega_S>>\omega_D$, eq.(28) reduces to eq.(24) devided by $\pi^{1/2}$. In this limit, I_j are analytically calculable, for example, $I_1=3/4$ and $I_2=15/8$. When $\omega_S=m\omega_D$, with m>>1 eq.(20) can be approximated by

$$\hat{q}_c=\frac{3\pi^{1/2}}{8m\varepsilon_n}(\eta_i+1-5\varepsilon_n) \qquad (29)$$

For m=3, as compared with the case of cut-off power spectrum given by eq.(25), the flux given by eq.(29) is smaller by a factor 2.

If we assume $\omega_S=\omega_*/\tau$, the spectrum width parameter becomes $(\omega_D/\omega_S)^2=4\varepsilon_n^2$. When $4\varepsilon_n^2<<1$, i.e., near the plasma edge, eq.(20) is approximated by

$$\hat{q}_c=\frac{3}{4}\pi^{1/2}(\eta_i+1-5\varepsilon_n) \qquad (30)$$

which is smaller by a factor $\pi^{1/2}$ as compared with the case of cut-off spectrum given by eq.(26). As seen in the above, the functional form of the flux $\hat{q}_C$ induced by the continuum C does not changes as we change the frequency power spectrum function $S(\omega)$. The functional form of $\hat{q}_C$, however, changes when we change the scaling of the width ω_S for the same function $S(\omega)$.

For the case $\omega_S=m\omega_D$, $\omega_S\to\infty$ as $r\to 0$ because ω_D is inversely proportional to r. In this case, the frequency power spectrum becomes white noise, i.e., no particular instability, and form eq.(20), the normalized flux $\hat{q}_C$ tends to zero at the center. This seems to be physically reasonable because there is no source of instability at the center. Near the plasma edge $r\to a$, on the other hand, the spectrum width ω_S becomes almost independent of r which

also seems to be consistent with experimental situations.

For the case of $\omega_s = \omega_*/\tau$. on the contrary, the spectrum width ω_s may be almost constant at the center r=0, because rL_n becomes a constant as $r \to 0$. Near the plasma edge, however, $\omega_s \to \infty$ since $L_n \to 0$ as $r \to a$, i.e., the power spectrum width sharply increases and tends to infinity, which is not likely to happen in experimental situations. The former case, $\omega_s = m\omega_D$, therefore, i.e., eq.(25) or eq.(29) may be more suitable for actual experimental situations.

If we introduce eq.(25) or eq.(29) into eq.(17), we have the continuum contribution to ion heat conductivity

$$\chi_i^c = \lambda \frac{v_i \rho_i^2}{R} \left(\frac{\eta_i + 1}{\varepsilon_n} - 5 \right) \qquad (31)$$

Expression (31) is equivalent to so called gyro-Bohm form: $\chi_i = \rho_i^2 v_i / L_n$. In this case the flux $\hat{q}_c$ and also the heat conductivity sharply increase near the edge. Substitutron of eq.(26) or eq.(30) into eq.(17) yields

$$\chi_i^c = \lambda \frac{v_i \rho_i^2}{R} (\eta_i + 1 - 5\varepsilon_n) \qquad (32)$$

We now evaluate the radial profiles of the normalized flux q and corresponding heat conductivity χ_i assuming simple parabolic type profiles, respectively, for density and temperature:

$$n = (n_o (1 - x^2)^{\alpha_n} + n_b) / (n_o + n_b) \qquad (33)$$

$$T_i = (T_o (1 - x^2)^{\alpha_T} + T_b) / (T_o + T_b) \qquad (34)$$

The variation of ion temperature profile as a function of profile parameter α_T is presented in Fig. 2 as a three dimensional surface graphics. The density profile n(x) as a function of α_n is exactly the same as $T_i(x)$ in Fig.2. The variation of the density profile parameter $\varepsilon_n(x)$ is also presented as a surface graphics in Fig. 3. The variaton of profile parameter $\eta_i(x)$ is presented as a surface graphics in Fig. 4a for $\alpha_n=0.5$, $n_b=0$ and $T_b=0.1$. When the density boundary balue is not zero, $n_b=0.1$, while the ion temperature boundary value is zero, $T_b=0$, the profile parameter η_i increases near the edge as shown in Fig. 4b.

The variation of normalized flux $\hat{q}_o$ by the discrete η_i-mode given

by eq.(12) is shown in Fig.5. The variation of normalized flux $\hat{q}_c$ due to the continuum contribution given by eq.(25) is also shown in Fig.6 for the same profile parameter α_n=0.5. The sharp increase of $\hat{q}_c$ near the periphery is due to the factor η_i/ε_n in eq.(25).

The ion heat conductivity χ_i has, as seen in eq.(14), the gyro-Bohm coefficient $\rho_i^2 v_i$ which is proportional to $T_i^{3/2}/B^2$. Due to the facter $T_i^{3/2}$, the ion heat conductivity χ_i usually sharply decreases as we go to the plasma edge, $r \to a$, when the variation $\hat{q}$ is mild. This is the case of χ_i^o given by eq.(15) as shown by a surface graphics in Fig.6. Due to the factor $T_i^{3/2}$, the peak in χ_i^o is shifted toward the center as compared with that of $\hat{q}_o$ as seen in Figs. 6 and 7. In the calculation of heat conductivity χ_i, the value of $\lambda\rho_i^2 v_i/R$ at the center is assumed to be unity($1m^2/sec$) in all cases. In the case of continuum contribution, χ_i^c given by eq.(32), however, increases sharply in the periphery as seen in Fig.8. In large tokamaks, experimentally observed heat conductivity in the L-mode discharge sharply increases in the periphery[3]. The continuum contribution presented in Fig.8 may, therefore, be applied for interpretation of the edge transport phenomenon observed in large tokamaks.

For the different boundary condition with n_b=0.1 and T_b=0, however, the variation of the heat conductivity χ_i^c changes as shown by the surface graphics in Fig. 9. Notice that the variation of χ_i^c near the edge changes depending on α_T as seen in Fig. 9, i.e., for small α_T χ_i^c shows the L-mode character, but for larger α_T, χ_i^c decreases toward the periphery which might corresponds to the case of high-Ti discharge in JT-60[3]. The surface graphics of χ_i^c with different scaling of the frequency power spectrum width given by eq.(32) is presented in Fig.10. The heat conductivity should always be positive. The negative χ_i^c in the above results came from the negative flux $\hat{q}_c$. The negative χ_i^c may, therefore, be interpreted as the inward ion flow.

So far the density profile parameter α_n is almost fixed at α_n=0.5. For larger α_n, the variation of heat conductivity χ_i^c in general is

nearly the same, but the magnitude of χ_i^C increases.

§5. Effect of Transit Resonance Continuum

In the previous sections, we neglected ion transit frequency $k_{\parallel} v_{\parallel}$ in the resonance denominator in eq.(1). In this section, we take into account the effect of transit ions. When both toroidal drift and transit effects are taken into account, the corresponding dispersion relation is described by the double integral form as given by eq.(4). Althought the transit ion is stabilizing when the transit time is shorter than the growth time of the discrete mode, the unstable η_i-mode exists[6][7] even when the transit effect presents.

When the transit frequency is introduced, the continuous eigenvalue spectrum induced by the resonance condition $\omega=\omega_D+k_{\parallel} v_{\parallel}$ extends to the whole real axis in the complex ω-plane. Due to the different velocity dependences of ω_D and $k_{\parallel} v_{\parallel}$, the continuum induced by this resonance has "multiplicity" in the negative real axis. To remove this complexity and concentrate to the transit resonance continuum effect, we neglect ω_D and consider the continuum induced by the resonance condition $\omega=k_{\parallel} v_{\parallel}$.

We evaluate the cross field ion thermal flux induced by this continuum. The normalized flux in eq.(8), in this case, may be written in the from

$$\hat{q}_c = \int_{-\infty}^{\infty} d\omega S(\omega)\pi \int d^3v (\omega-\omega_*) J_o^2(\alpha) F_M \frac{E}{T} \delta(\omega^2 - k_{\parallel}^2 v_{\parallel}^2) \qquad (35)$$

Carrying out the velocity space integration for the Maxwellian plasma, we have

$$\hat{q}_c = \frac{1}{\pi^{1/2}} \int_{-\infty}^{\infty} dw S(\omega) (\omega + \frac{\omega_*}{\tau}) e^{-w^2} \left\{ w^2 \Gamma_o + \Gamma_o + b(\Gamma_1 - \Gamma_o) \right\} \qquad (36)$$

where $w=\omega/\omega_t$ and $\eta_i=0$ is also assumed for the sake of simplicity. When $S(\omega)$ is even, the first term ω in the brackets in eq.(3) vanishes.

For the cut-off power spectrum, eq.(36) reduces to

$$q_c = \frac{\omega_*}{2\tau\omega_s}\left[\left(\frac{3}{2}\Gamma_o(b) + b(\Gamma_1 - \Gamma_o)\right)\Phi\left(\frac{\omega_s}{\omega_t}\right) - 2\frac{\omega_s}{\omega_t}e^{-\left(\frac{\omega_s}{\omega_t}\right)^2}\right] \qquad (37)$$

where $\Gamma_n(b) = I_n(b)\exp(-b)$, I_n is the modified Bessel function, and Φ is the probability function defined by

$$\Phi(z) = \frac{2}{\pi^{1/2}}\int_o^z dt e^{-t^2}$$

When the spectrum width is large as compared with the ion transit frequency: $\omega_s >> \omega_t$, Φ tends to unity, and eq.(37) reduces to

$$\hat{q}_c = \frac{\omega_*}{2\tau\omega_s}\left\{\frac{3}{2}\Gamma_o(b) + b(\Gamma_1 - \Gamma_o)\right\} \qquad (38)$$

In the white noise limit $\omega_s \to \infty$, $\hat{q}_c \to 0$. Introducing eq.(38) into eq.(17), we have for $b<<1$

$$\chi_i^c = \lambda\frac{\rho_i^2 v_i}{R}\cdot\frac{\omega_*}{\tau\omega_s}\left(1 - \frac{5}{3}b\right) \qquad (39)$$

In this case too, the scaling changes depending on how we choose the frequency power spectrum width parameter ω_s. If we choose $\omega_s = m\omega_D$, χ_i^c increases sharply toward the periphery as in the case of the toroidal drift resonance.

§6. Summary and Discussion

The cross field ion thermal fluxes due to the ion temperature gradient mode and the continuous eigenvalue spectrum induced by the toroidal ion drift resonance have been evaluated by assuming the toroidal ion drift frequency ω_D is proportional to ion energy E.

Assuming the relation $|e\phi/T_i|^2 = S(\omega)/k_\perp^2 L^2$ with $L^2 = RL_T$ and $k_\perp\rho_i = \text{const.}$, the ion heat conductivity χ_i is expressed in term of the gyro-Bohm coefficient with the normalized flux $\hat{q}$ as given by eq.(14). Since χ_i^o induced by the discrete η_i-mode as given by eq.(15) is peaked in the intermediate region as seen in Fig. 7, the discrete η_i-mode may be applicable to the interpretation of of experimental observations at least in the intermediate region[3]. On the other hand, χ_i^c

induced by the continuum contribution as given by eq.(31) increases sharply toward the edge, eq.(31) may be applicable to the interpretation of the experimental observation, sharp increase of χ_i, in the periphery. In the central region, the ion heat conductivity given by the neoclassical theoy may be applicable.

The profile of χ_i strictly depends on the assumptions we have made. The most important assumtion for the profile of χ_i is the characteristic scale lenght L. If we assume $L^2=L_nL_T$, eq.(14) changes to

$$\chi_i=\lambda\frac{\rho_i^2 v_i}{R}\cdot\frac{\hat{q}}{\varepsilon_n} \qquad (40)$$

While if $L=L_n$ is assumed as in usual theory, eq.(14) is transformed to

$$\chi_i=\lambda\frac{\rho_i^2 v_i}{R}\cdot\frac{\hat{q}}{\varepsilon_n\eta_i} \qquad (41)$$

If we apply eq.(40) or eq.(41), due to the factor $1/\varepsilon_n$, χ_i may sharply increase in the periphery. The assumption that $k_\perp\rho_i$=const. independent of r also contradicts with the variation of T_i, because ρ_i is proportional to $T_i^{1/2}/B$. The functional form of $\hat{q}_c$ also depends on the scaling of the width of frequency power spectrum function $S(\omega)$, as shown in eqs.(31) and (32).

The gyro-Bohm coefficient $v_i\rho_i^2/R$ is used in common to express the ion heat conductivities (15), (31) and (39), respectively induced by the discrete η_i-mode, toroidal drift resonance continuum and transit resonance continuum. This coefficient is derived under the assumptions of $k_\perp\rho i$=const. and $L=RL_T$ as mentioned in the above. Without these assumptions, χ_i can be expressed by $\chi_i=D_B/k_\perp L$ where $D_B=cT/eB$ is the Bohm diffusion coefficient. If we assume $S(\omega)=1$, this expression can be rewritten by

$$\chi_i=\left|\frac{e\phi}{T}\right|D_B$$

This expression is the same as the upper bound of the diffusion coefficient due to electrostatic turbulence derived by the resonance broadening nonlinear treatment[17].

Acknowledgement

This study was a joint research programme with the National Institute for Fusion Science.

References

(1) S.Ejima,T.W.Petrie,A.C.Riviere,et.al.,Nucl.Fusion,**22**(1982)1627.

(2) R.J.Groebner,W.Peiffer,F.C.Blau,et al.,Nucl.,Fusion,**26**(1986)543.

(3) H.Shirai, T.Hirayama, Y.Koide, M.Azumi, D.R. Mikelsen, S.D.Scott, Ion Temperature Profile Simulation of JT-60 and TFTR Plasmas with Ion Temperature Gradient Mode, submitted to Nucl. Fusion.

(4) H.Nordman,J.Wieland, Nucl.Fusion,**29**(1989)251.

(5) F.Romanelli, Phys.Fluids, **B1**(1989)1018.

(6) F.Romanelli and Briguglio, Phys.Fluids **B2**(1990)754.

(7) J.Q.Dong, W.Horton and J.Y.Kim, Phys.Fluids **B4**(1992)1867.

(8) A.Hirose, Phys. Fluids,**B5**(1993)320.

(9) T.H.Dupree, Phys. Fluids,**10**(1967)1049.

(10) N.G.Van Kampen and B.V.Felderhof,*Theoretical Methods in Plasma Physics* (translated into Japanese by M. Nishida) Kinokuniya, Tokyo p.153,1973.

(11) K.M.Case and P.F.Zweifel, *Linear Transport Theory*, Addison-Wesley, New York, 1967.

(12) T.Yamagishi, Transport Theory and Statistical Physics,3(1973)107.

(13) T.Yamagishi, *Cross Field Energy Flux due to Ion Temperature Gradient Mode in a Tokamak*, US-Japan Workshop on η_i-mode and turbulent transport, University of Texas, 1993.

(14) T.Antonsen, B.Coppi, R.Englade, Nucl.Fusion,**19**(1979)641.

(15) T.Yamagishi, Phys. Fluids, **22**(1979)2431.

(16) A.J.Wooton,H.Y.Tsui and S.Prager,Plasma Physics and Contr. Fusion, **34**(1992)2023.

(17) T.Yamagishi,J.Plasma Physics, 36(1986)281.

Figures Captions

Fig. 1: Variation of discrete η_i-mode eigenvalue in the complex ω-plane for ω_t=0, b=0, and various values of ε_n and η_i.

Fig.2: Surface graphics of ion temperature profile as a function of profile parameter α_T for T_b=0.

Fig.3: Surface graphics of ε_n-profile as a function of profile parameter α_n for n_b=0 and ε=0.29.

Fig.4a: Surface graphics of η_i-profile as a function of profile parameter α_T for α_n=0.5, n_b=0 and T_b=0.1.

Fig.4b: Surface graphics of η_i-profile as a function of profile parameter α_T for α_n=0.5, n_b=0.1 and T_b=0.1.

Fig.5: Surface graphics of normalized flux $\hat{q}_o$ due to discrete η_i-mode as a function of profile parameter α_T for α_n=0.5, n_b=0. and T_b=0.1.

Fig.6: Surface graphics of normalized flux $\hat{q}_c$ due to continuum contribution as a function of profile parameter α_T for α_n=0.5, n_b=0. and T_b=0.1.

Fig.7: Surface graphics of ion heat conductivity χ_i^o due to discrete η_i-mode as a function of profile parameter α_T for α_n=0.5, n_b=0 and T_b=0.1.

Fig.8: Surface graphics of ion heat conductivity χ_i^c due to continuum contribution as a function of profile parameter α_T for α_n=0.5, n_b=0 and T_b=0.1

Fig.9: Surface graphics of ion heat conductivity χ_i^c due to continuum contribution for α_n=0.5, T_b=0 and n_b=0.1.

Fig.10: Surface graphics of ion heat conductivity χ_i^c due to continuum contribution with $\omega_s=\omega^*$ for α_n=0.5, T_b=0 and n_b=0.1.

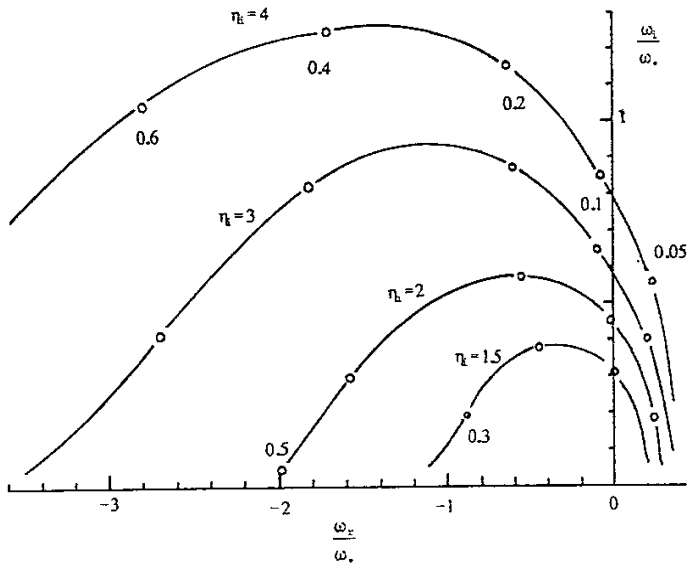

Fig. 1

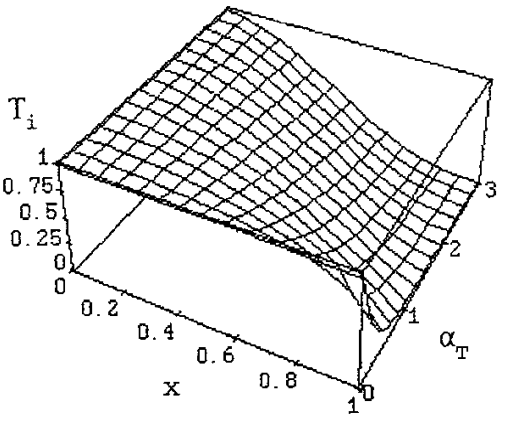

Fig. 2

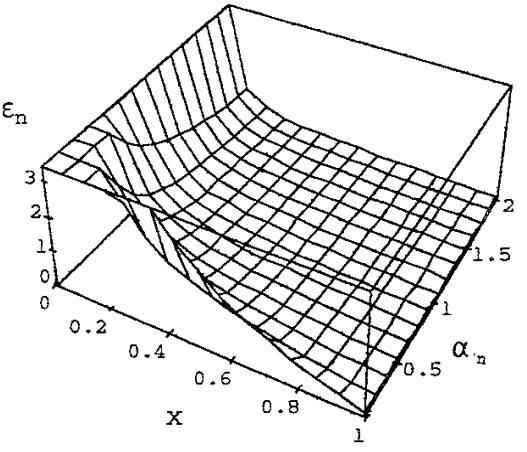

Fig. 3

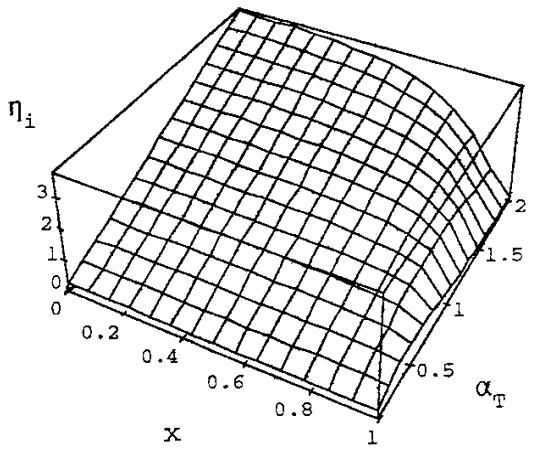

Fig.4a

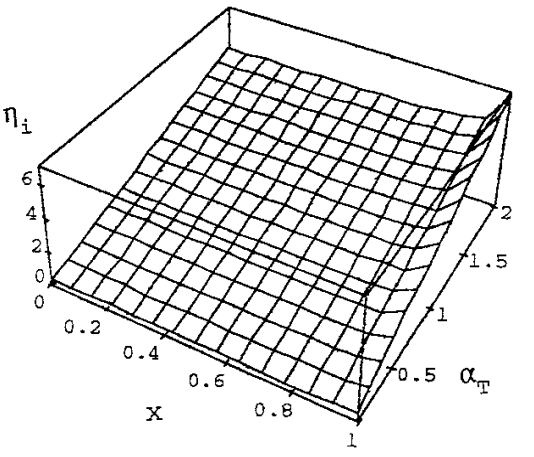

Fig. 4b

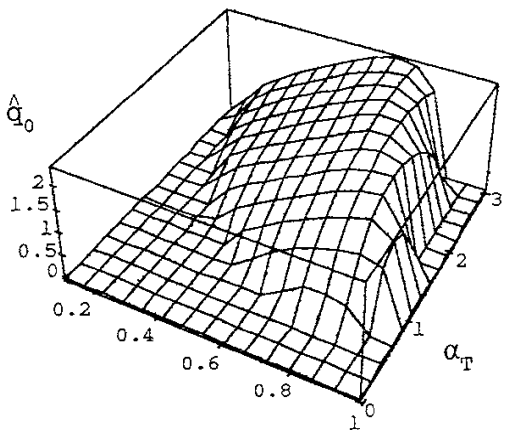

Fig. 5

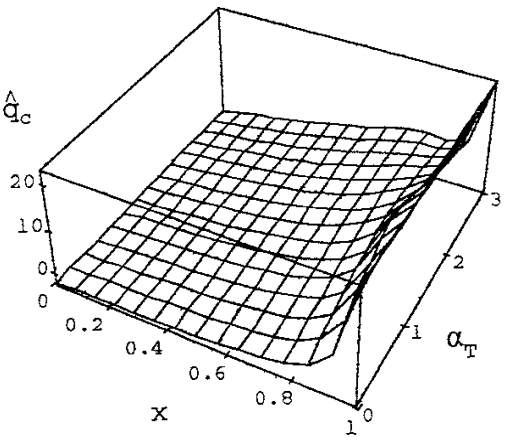

Fig. 6

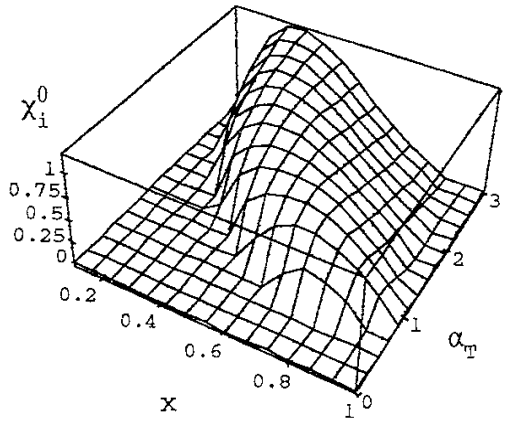

Fig. 7

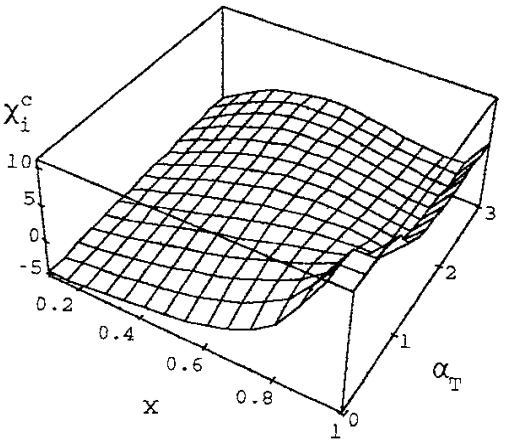

Fig. 8

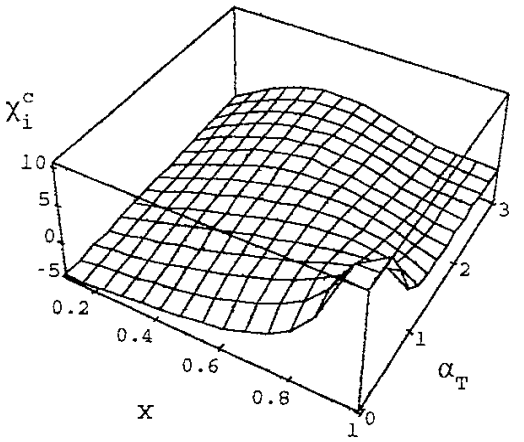

Fig. 9

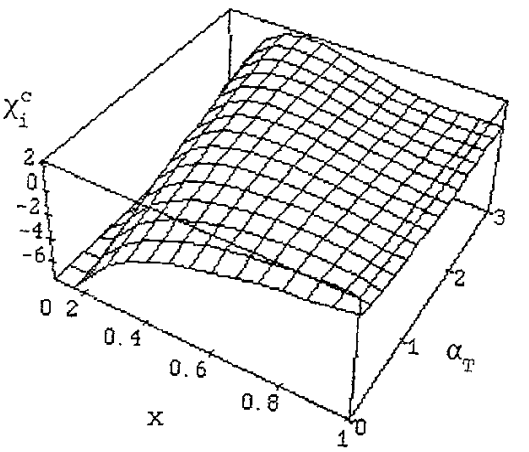

Fig. 10

Recent Issues of NIFS Series

NIFS-170 H. Sugama, M. Okamoto and M. Wakatani, *K- ε Model of Anomalous Transport in Resistive Interchange Turbulence* ; Sep, 1992

NIFS-171 H. Sugama, M. Okamoto and M. Wakatani, *Vlasov Equation in the Stochastic Magnetic Field* ; Sep. 1992

NIFS-172 N. Nakajima, M. Okamoto and M. Fujiwara, *Physical Mechanism of E_ψ-Driven Current in Asymmetric Toroidal Systems* ; Sep.1992

NIFS-173 N. Nakajima, J. Todoroki and M. Okamoto, *On Relation between Hamada and Boozer Magnetic Coordinate System* ; Sep. 1992

NIFS-174 K. Ichiguchi, N. Nakajima, M. Okamoto, Y. Nakamura and M. Wakatani, *Effects of Net Toroidal Current on Mercier Criterion in the Large Helical Device* ; Sep. 1992

NIFS-175 S. -I. Itoh, K. Itoh and A. Fukuyama, *Modelling of ELMs and Dynamic Responses of the H-Mode* ; Sep. 1992

NIFS-176 K. Itoh, S.-I. Itoh, A. Fukuyama, H. Sanuki, K. Ichiguchi and J. Todoroki, *Improved Models of β-Limit, Anomalous Transport and Radial Electric Field with Loss Cone Loss in Heliotron / Torsatron* ; Sep. 1992

NIFS-177 N. Ohyabu, K. Yamazaki, I. Katanuma, H. Ji, T. Watanabe, K. Watanabe, H. Akao, K. Akaishi, T. Ono, H. Kaneko, T. Kawamura, Y. Kubota, N. Noda, A. Sagara, O. Motojima, M. Fujiwara and A. Iiyoshi, *Design Study of LHD Helical Divertor and High Temperature Divertor Plasma Operation* ; Sep. 1992

NIFS-178 H. Sanuki, K. Itoh and S.-I. Itoh, *Selfconsistent Analysis of Radial Electric Field and Fast Ion Losses in CHS Torsatron / Heliotron* ; Sep. 1992

NIFS-179 K. Toi, S. Morita, K. Kawahata, K. Ida, T. Watari, R. Kumazawa, A. Ando, Y. Oka, K. Ohkubo, Y. Hamada, K. Adati, R. Akiyama, S. Hidekuma, S. Hirokura, O. Kaneko, T. Kawamoto, Y. Kawasumi, M. Kojima, T. Kuroda, K. Masai, K. Narihara, Y. Ogawa, S. Okajima, M. Sakamoto, M. Sasao, K. Sato, K. N. Sato, T. Seki, F. Shimpo, S. Tanahashi, Y. Taniguchi, T. Tsuzuki, *New Features of L-H Transition in Limiter H-Modes of JIPP T-IIU* ; Sep. 1992

NIFS-180 H. Momota, Y. Tomita, A. Ishida, Y. Kohzaki, M. Ohnishi, S. Ohi, Y. Nakao and M. Nishikawa, *D-^{3}He Fueled FRC Reactor "Artemis-L"*

; Sep. 1992

NIFS-181 T. Watari, R. Kumazawa, T. Seki, Y. Yasaka, A. Ando, Y. Oka,O. Kaneko, K. Adati, R. Akiyama, Y. Hamada, S. Hidekuma, S. Hirokura, K. Ida, K. Kawahata, T. Kawamoto, Y. Kawasumi, S. Kitagawa, M. Kojima, T. Kuroda, K. Masai, S. Morita, K. Narihara, Y. Ogawa, K. Ohkubo, S. Okajima, T. Ozaki, M. Sakamoto, M. Sasao, K. Sato, K. N. Sato, F.Shimpo, H. Takahashi, S. Tanahasi, Y. Taniguchi, K. Toi, T. Tsuzuki and M. Ono, *The New Features of Ion Bernstein Wave Heating in JIPP T-IIU Tokamak* ;Sep, 1992

NIFS-182 K. Itoh, H. Sanuki and S.-I. Itoh, *Effect of Alpha Particles on Radial Electric Field Structure in Torsatron / Heliotron Reactor*; Sep. 1992

NIFS-183 S. Morimoto, M. Sato, H. Yamada, H. Ji, S. Okamura, S. Kubo, O. Motojima, M. Murakami, T. C. Jernigan, T. S. Bigelow, A. C. England, R. S. Isler, J. F. Lyon, C. H. Ma, D. A. Rasmussen, C. R. Schaich, J. B. Wilgen and J. L. Yarber, *Long Pulse Discharges Sustained by Second Harmonic Electron Cyclotron Heating Using a $35GH_Z$ Gyrotron in the Advanced Toroidal Facility*; Sep. 1992

NIFS-184 S. Okamura, K. Hanatani, K. Nishimura, R. Akiyama, T. Amano, H. Arimoto, M. Fujiwara, M. Hosokawa, K. Ida, H. Idei, H. Iguchi, O. Kaneko, T. Kawamoto, S. Kubo, R. Kumazawa, K. Matsuoka, S. Morita, O. Motojima, T. Mutoh, N. Nakajima, N. Noda, M. Okamoto, T. Ozaki, A. Sagara, S. Sakakibara, H. Sanuki, T. Seki, T. Shoji, F. Shimbo, C. Takahashi, Y. Takeiri, Y. Takita, K. Toi, K. Tsumori, M. Ueda, T. Watari, H. Yamada and I. Yamada, *Heating Experiments Using Neutral Beams with Variable Injection Angle and ICRF Waves in CHS* ; Sep. 1992

NIFS-185 H. Yamada, S. Morita, K. Ida, S. Okamura, H. Iguchi, S. Sakakibara, K. Nishimura, R. Akiyama, H. Arimoto, M. Fujiwara, K. Hanatani, S. P. Hirshman, K. Ichiguchi, H. Idei, O. Kaneko, T. Kawamoto, S. Kubo, D. K. Lee, K. Matsuoka, O, Motojima, T. Ozaki, V. D. Pustovitov, A. Sagara, H. Sanuki, T. Shoji, C. Takahashi, Y. Takeiri, Y. Takita, S. Tanahashi, J. Todoroki, K. Toi, K. Tsumori, M. Ueda and I. Yamada, *MHD and Confinement Characteristics in the High-β Regime on the CHS Low-Aspect-Ratio Heliotron / Torsatron* ; Sep. 1992

NIFS-186 S. Morita, H. Yamada, H. Iguchi, K. Adati, R. Akiyama, H. Arimoto, M. Fujiwara, Y. Hamada, K. Ida, H. Idei, O. Kaneko, K. Kawahata, T. Kawamoto, S. Kubo, R. Kumazawa, K. Matsuoka, T. Morisaki, K. Nishimura, S. Okamura, T. Ozaki, T. Seki, M. Sakurai, S, Sakakibara, A. Sagara, C. Takahashi, Y. Takeiri, H. Takenaga, Y. Takita, K. Toi, K. Tsumori, K. Uchino, M. Ueda, T. Watari, I. Yamada, *A Role of Neutral Hydrogen in CHS Plasmas with Reheat and Collapse and Comparison with JIPP T-IIU Tokamak Plasmas* ; Sep. 1992

NIFS-187 K. Ioth, S.-I. Itoh, A. Fukuyama, M. Yagi and M. Azumi, *Model of the L-Mode Confinement in Tokamaks* ; Sep. 1992

NIFS-188 K. Itoh, A. Fukuyama and S.-I. Itoh, *Beta-Limiting Phenomena in High-Aspect-Ratio Toroidal Helical Plasmas*; Oct. 1992

NIFS-189 K. Itoh, S. -I. Itoh and A. Fukuyama, *Cross Field Ion Motion at Sawtooth Crash* ; Oct. 1992

NIFS-190 N. Noda, Y. Kubota, A. Sagara, N. Ohyabu, K. Akaishi, H. Ji, O. Motojima, M. Hashiba, I. Fujita, T. Hino, T. Yamashina, T. Matsuda, T. Sogabe, T. Matsumoto, K. Kuroda, S. Yamazaki, H. Ise, J. Adachi and T. Suzuki, *Design Study on Divertor Plates of Large Helical Device (LHD)* ; Oct. 1992

NIFS-191 Y. Kondoh, Y. Hosaka and K. Ishii, *Kernel Optimum Nearly-Analytical Discretization (KOND) Algorithm Applied to Parabolic and Hyperbolic Equations* : Oct. 1992

NIFS-192 K. Itoh, M. Yagi, S.-I. Itoh, A. Fukuyama and M. Azumi, *L-Mode Confinement Model Based on Transport-MHD Theory in Tokamaks* ; Oct. 1992

NIFS-193 T. Watari, *Review of Japanese Results on Heating and Current Drive* ; Oct. 1992

NIFS-194 Y. Kondoh, *Eigenfunction for Dissipative Dynamics Operator and Attractor of Dissipative Structure* ; Oct. 1992

NIFS-195 T. Watanabe, H. Oya, K. Watanabe and T. Sato, *Comprehensive Simulation Study on Local and Global Development of Auroral Arcs and Field-Aligned Potentials* ; Oct. 1992

NIFS-196 T. Mori, K. Akaishi, Y. Kubota, O. Motojima, M. Mushiaki, Y. Funato and Y. Hanaoka, *Pumping Experiment of Water on B and LaB_6 Films with Electron Beam Evaporator* ; Oct., 1992

NIFS-197 T. Kato and K. Masai, *X-ray Spectra from Hinotori Satellite and Suprathermal Electrons* ; Oct. 1992

NIFS-198 K. Toi, S. Okamura, H. Iguchi, H. Yamada, S. Morita, S. Sakakibara, K. Ida, K. Nishimura, K. Matsuoka, R. Akiyama, H. Arimoto, M. Fujiwara, M. Hosokawa, H. Idei, O. Kaneko, S. Kubo, A. Sagara, C. Takahashi, Y. Takeiri, Y. Takita, K. Tsumori, I. Yamada and H. Zushi, *Formation of H-mode Like Transport Barrier in the CHS Heliotron / Torsatron* ; Oct. 1992

NIFS-199 M. Tanaka, *A Kinetic Simulation of Low-Frequency Electromagnetic Phenomena in Inhomogeneous Plasmas of Three-Dimensions* ; Nov. 1992

NIFS-200 K. Itoh, S.-I. Itoh, H. Sanuki and A. Fukuyama, *Roles of Electric Field on Toroidal Magnetic Confinement*, Nov. 1992

NIFS-201 G. Gnudi and T. Hatori, *Hamiltonian for the Toroidal Helical Magnetic Field Lines in the Vacuum*; Nov. 1992

NIFS-202 K. Itoh, S.-I. Itoh and A. Fukuyama, *Physics of Transport Phenomena in Magnetic Confinement Plasmas*; Dec. 1992

NIFS-203 Y. Hamada, Y. Kawasumi, H. Iguchi, A. Fujisawa, Y. Abe and M. Takahashi, *Mesh Effect in a Parallel Plate Analyzer*; Dec. 1992

NIFS-204 T. Okada and H. Tazawa, *Two-Stream Instability for a Light Ion Beam -Plasma System with External Magnetic Field;* Dec. 1992

NIFS-205 M. Osakabe, S. Itoh, Y. Gotoh, M. Sasao and J. Fujita, *A Compact Neutron Counter Telescope with Thick Radiator (Cotetra) for Fusion Experiment*; Jan. 1993

NIFS-206 T. Yabe and F. Xiao, *Tracking Sharp Interface of Two Fluids by the CIP (Cubic-Interpolated Propagation) Scheme*, Jan. 1993

NIFS-207 A. Kageyama, K. Watanabe and T. Sato, *Simulation Study of MHD Dynamo : Convection in a Rotating Spherical Shell*; Feb. 1993

NIFS-208 M. Okamoto and S. Murakami, *Plasma Heating in Toroidal Systems*; Feb. 1993

NIFS-209 K. Masai, *Density Dependence of Line Intensities and Application to Plasma Diagnostics*; Feb. 1993

NIFS-210 K. Ohkubo, M. Hosokawa, S. Kubo, M. Sato, Y. Takita and T. Kuroda, *R&D of Transmission Lines for ECH System* ; Feb. 1993

NIFS-211 A. A. Shishkin, K. Y. Watanabe, K. Yamazaki, O. Motojima, D. L. Grekov, M. S. Smirnova and A. V. Zolotukhin, *Some Features of Particle Orbit Behavior in LHD Configurations*; Mar. 1993

NIFS-212 Y. Kondoh, Y. Hosaka and J.-L. Liang, *Demonstration for Novel Self-organization Theory by Three-Dimensional Magnetohydrodynamic Simulation*; Mar. 1993

NIFS-213 K. Itoh, H. Sanuki and S.-I. Itoh, *Thermal and Electric Oscillation Driven by Orbit Loss in Helical Systems*; Mar. 1993